Angle-dependent magnetoresistance oscillations of cuprate superconductors in a model with Fermi surface reconstruction and magnetic breakdown

Sylvia K. Lewin[*] and James G. Analytis

Department of Physics, University of California, Berkeley, California 94720, USA

and Materials Sciences Division, Lawrence Berkeley National Laboratory, Berkeley, California 94720, USA

We calculate angle-dependent magnetoresistance oscillations (AMRO) for interlayer transport of cuprate superconductors in the presence of (π,π) order. The order reconstructs the Fermi surface, creating magnetic breakdown junctions; we show how such magnetic breakdown effects can be incorporated into calculations of interlayer conductivity for this system. We successfully fit experimental data from an overdoped cuprate using our model, showing that behavior previously attributed to anisotropic scattering in this material may in fact be due to (π,π) ordering. This work paves the way for the use of AMRO as a tool to distinguish ordered states that have different ordering wave vectors.

I. INTRODUCTION

Understanding the nature of broken symmetry phases in the thermodynamic phase diagram of the cuprates is a key step toward understanding the origin of high-temperature superconductivity. For example, the discovery of the pseudogap [1] has fueled the search for many kinds of order [2–7], including nematic phases that could strongly enhance T_c [8]. Yet of the broken symmetries connected to unconventional superconductivity, antiferromagnetism remains one of the most important, appearing in cuprate, iron-pnictide, organic, and heavy fermion materials [9–11].

Evidence of Fermi surface reconstruction arising from broken symmetry order has come from quantum oscillation measurements in both hole-doped [12–14] and electron-doped [15] cuprates at low temperatures and high magnetic fields, but the nature of the broken symmetry remains a matter of considerable debate. Antiferromagnetic (π,π) reconstruction has been proposed for both the hole- and electron-doped materials [15,16], but recent evidence for a (possibly field-induced) charge density wave [17–20] has suggested more complex orders are driving the reconstruction.

The ability to experimentally differentiate between these different ordered states is crucial. In this work, we suggest that interlayer angle-dependent magnetoresistance oscillations (AMRO) can be used to distinguish between long-range ordered states in the cuprates that have different ordering wave vectors. Angle-dependent magnetoresistance is a sensitive probe of the Fermi surface of a material [21–25] and can therefore be used to investigate the geometry of a reconstructed Fermi surface. The measurement is also sensitive to the energy scale of any (translational) symmetry-breaking order [26]. This energy scale is related to a "magnetic breakdown field," as we describe below. Importantly, these effects on AMRO can be observed even in materials that do not show quantum oscillations. Thus the measurement is useful in systems in which sample disorder is high, or in which the order has a small correlation length [5,6].

AMRO data from $Tl_2Ba_2CuO_{6+\delta}$ provided the earliest transport evidence for the existence of a three-dimensional Fermi surface in an overdoped cuprate [21]. The temperature evolution of the AMRO is consistent with a superposition of isotropic and anisotropic scattering rates about the Fermi surface [27], and it was determined that these do not have the same temperature dependence: the isotropic scattering rate is quadratic with temperature (as expected of an ordinary Fermi liquid), while the anisotropic scattering rate is linear (connecting it to the non-Fermi liquid physics of the cuprate phase diagram). Additionally, the anisotropic scattering is strongest in the antinodal region of the Fermi surface. Therefore it has been suggested that the anomalous scattering temperature dependence may be related to (π,π) fluctuations [27–29], possibly originating from antiferromagnetism. A similar anomalous scattering has been observed in overdoped $La_{2-x}Sr_xCuO_4$ through angle-resolved photoemission spectroscopy measurements and has been posited to arise from antiferromagnetic fluctuations in that material [30]. We show here that the introduction of (π,π) order on the Fermi surface of $Tl_2Ba_2CuO_{6+\delta}$ will indeed affect the AMRO of this system in a similar way to the introduction of anisotropic scattering.

We demonstrate this connection by simulating the AMRO of a model cuprate material in the presence of antiferromagnetic order. The interpretation of AMRO measurements requires efficient and versatile calculations of the magnetotransport of a given Fermi surface so that models can be compared to experimental results. These calculations are more challenging in the presence of static order that reconstructs the Fermi surface. We have developed a general method to perform such calculations for quasi-two-dimensional (Q2D) materials based on previous work in organic metals [31]. It is both easy to implement and computationally inexpensive. In Sec. II we use this method to calculate the interlayer magnetoresistance of a tetragonal Q2D material in the presence of (π,π) order and including the effects of magnetic breakdown. In Sec. III we apply this model to the known Fermi surface of $Tl_2Ba_2CuO_{6+\delta}$[21] and show that the temperature dependence of the AMRO can be captured by this magnetic breakdown model. In Sec. IV we discuss the physical consequences of this model and its potential range of applicability for distinguishing between different kinds of broken symmetry

---

*Corresponding author: sylviakl@berkeley.edu

order in the cuprates. Our general method is laid out in detail in Appendix A.

II. AMRO IN THE PRESENCE OF (π,π) ORDER

As a first application of our method, we wish to understand how the AMRO of the cuprates is affected by antiferromagnetism. We therefore consider the case of a Q2D tetragonal material under static (π,π) antiferromagnetic order, though noting that the model below does not depend on the origin of the (π,π) order. As shown in Fig. 1(a), the original Brillouin zone of such a material will have a square cross section with primitive reciprocal lattice vectors along k_x and k_y; we define all azimuthal angles in this paper with respect to k_x. In the presence of (π,π) order, the Brillouin zone is halved in cross section, resulting in a reconstruction of the Fermi surface as shown in Figs. 1(b) and 1(c). This new reconstructed Brillouin zone will have primitive reciprocal lattice vectors along k_x' and k_y', which are rotated by 45° with respect to k_x and k_y.

Quasiparticles traversing the Fermi surface will Bragg diffract at the reconstructed Brillouin zone boundaries, so they will travel along three distinct Fermi surface pockets as shown in Fig. 1(d). However, in a large magnetic field, the quasiparticle path in real space may be curved sufficiently to avoid Bragg diffraction. This is known as *magnetic breakdown*
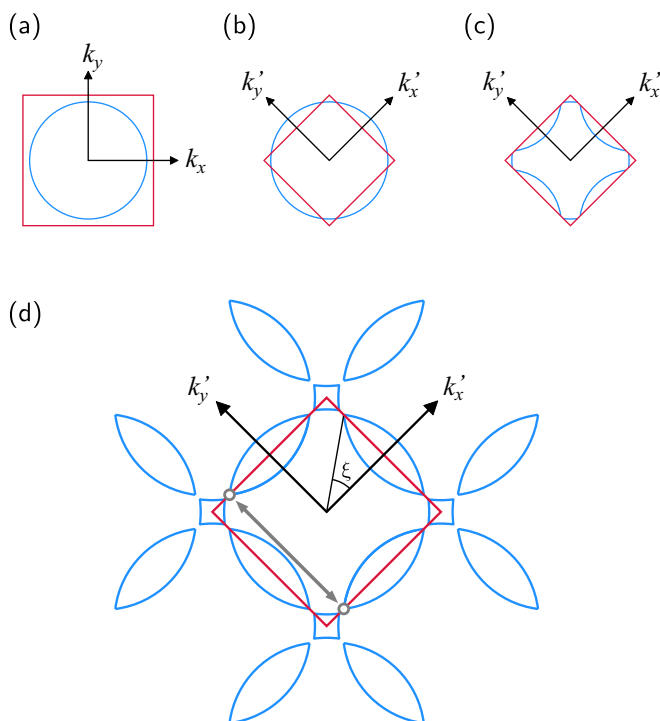

(a)   (b)   (c)

(d)

FIG. 1. (Color online) Fermi surface reconstruction of a Q2D material under (π, π) antiferromagnetic order, as viewed along k_z. (a) The Fermi surface (FS) and first Brillouin zone (BZ) of a Q2D tetragonal material; (b) the reconstructed BZ and (c) reconstructed FS of the material following the onset of (π,π) antiferromagnetic order; (d) the repeated-zone view of the reconstructed FS, illustrating the small cross sections of FS that have replaced the unreconstructed cylindrical FS. The gray line illustrates Bragg diffraction between two magnetic breakdown junctions at the BZ boundary. The angle ξ is also defined here; it will be used in our conductivity calculations.

(MB) and can be thought of as a tunneling in k space from one pocket to the next [26]. The probability to tunnel in this way is given by $p = e^{-B_0/B}$, where B_0 is the breakdown field and is a material-dependent constant proportional to the gap in k space between Fermi surface sections [32]. At every instance the quasiparticle path reaches a Brillouin zone boundary, the quasiparticle may either Bragg diffract or undergo MB; thus such points in the quasiparticle path are known as MB junctions. As can be seen in Fig. 1(d), the system in question has eight MB junctions.

We must take the effect of these MB junctions into account when calculating conductivity. The conductivity of a Q2D material in a magnetic field can be calculated using the Shockley tube integral form of the Boltzmann transport equation [33],

$$\sigma_{\alpha\beta} = \frac{e^2}{4\pi^3\hbar^2}\frac{m^*}{\omega_c}\int dk_B \int_0^{2\pi} v_\alpha(\varphi_0,k_B)d\varphi_0$$
$$\times \int_{\varphi_0}^{\infty} v_\beta(\varphi,k_B)e^{-(\varphi-\varphi_0)/\omega_c\tau}d\varphi, \qquad (1)$$

where φ_0 is the initial azimuthal position of the quasiparticle and φ is its position after some time t has passed [34]. The effective mass of the quasiparticle is represented by m^* and the cyclotron frequency is $\omega_c = eB/m^*$. The velocities in Eq. (1) are Fermi velocities.

The vector $\boldsymbol{k}_B$ points parallel to the magnetic field and defines the orbital path of a quasiparticle. We integrate across all values of its magnitude. For a given magnitude, the tip of the vector will touch a single quasiparticle orbit which can be defined by k_z^0, the k_z position of the orbital plane at the center of the Fermi surface (see Fig. 2). The magnetic field's direction is defined by a polar angle (θ) with respect to k_z and an azimuthal angle (ϕ) with respect to k_x. We can write $|\boldsymbol{k}_B| = k_z^0\cos(\theta)$ and therefore convert our integral over $\boldsymbol{k}_B$ to one over k_z^0.

Note that both m^* and ω_c depend on the orientation of the applied magnetic field. Specifically, $m^* = m_0^*/\cos(\theta)$ and $\omega_c = \omega_0\cos(\theta)$, where m_0^* and ω_0 are the cyclotron effective mass and cyclotron frequency at $\theta = 0$ [35].

Since AMRO is a probe of interlayer conductivity, we want to calculate σ_{zz}. This means we need an expression for v_z, which we can obtain from a symmetry-constrained model of the Fermi surface. The following equation describes a Q2D Fermi surface of a layered tetragonal material with simple cosine warping along k_z [21,36]:

$$E_F(k_z,\varphi) = \frac{\hbar^2 k_F^{\|2}(\varphi)}{2m^*} - \frac{2t_\perp a}{\pi}\cos\left(\frac{k_z c}{2}\right)F(\varphi). \qquad (2)$$

In the above, $t_\perp$ is the interlayer hopping, while $k_F^{\|}(\varphi)$ and $F(\varphi)$ parameterize the Fermi surface in the azimuthal cylindrical coordinate. The in-plane and out-of-plane lattice parameters are denoted by a and c, respectively. Using $v_z = \frac{1}{\hbar}\frac{dE(k)}{dk_z}$, we find the interlayer velocity to be

$$v_z(\boldsymbol{k},\varphi) = \frac{t_\perp ac}{\pi\hbar}\sin\left(\frac{k_z c}{2}\right)F(\varphi). \qquad (3)$$

When a quasiparticle Bragg diffracts at the Brillouin zone boundary it will have a momentum change given by a
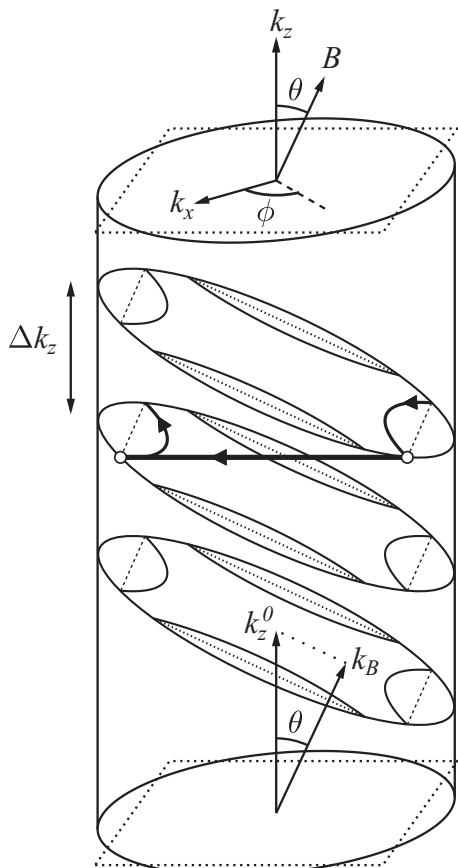
FIG. 2. When a magnetic field is applied to a Q2D material, quasiparticles will trace out orbits on the cylindrical Fermi surface that are perpendicular to the applied field. On the lowest orbit in this figure, we define the parameters k_z^0 and k_B. On the upper two orbits, we illustrate the fact that a quasiparticle undergoing Bragg diffraction moves to a different cross section of the Fermi surface. The dashed lines represent the Brillouin zone boundaries for the reconstructed Fermi surface. Note that the azimuthal angle ϕ is defined with respect to k_x of the *unreconstructed* system.

reciprocal lattice vector, so its momentum in the z direction will not change. The quasiparticle will jump to a different "slice" of the Fermi surface [31], changing its value of k_z^0 but preserving k_z (see Fig. 2). The amount by which k_z^0 changes after Bragg diffraction depends on which MB junctions are involved; for each pair of MB junctions, the value of Δk_z can be calculated using purely geometric means (see Appendix C). Therefore we can see that for a given quasiparticle

$$k_z(\varphi) = k_z^0 - k_F^{\parallel}(\varphi)\tan(\theta)\cos(\varphi - \phi) + \sum_{j=1}^{8} n_j(\varphi)\Delta k_z^{(j)}, \quad (4)$$

where $\Delta k_z^{(j)}$ is the amount by which k_z^0 changes each time the quasiparticle Bragg diffracts from the jth MB junction, and n_j is the number of times Bragg diffraction occurs from that junction [31]. Note that we have neglected the influence of the interlayer warping on particle motion; we assume the interlayer warping is much weaker than the in-plane warping, so this is a reasonable omission except for $\theta \approx 90°$. Setting

$n_j(\varphi_0) = 0$ we find

$$\sigma_{zz} = \frac{m^*\cos(\theta)}{\omega_c}\int_{-2\pi/c}^{2\pi/c}dk_z^0\int_0^{2\pi}d\varphi_0\,F(\varphi_0)\sin\left[\frac{ck_z(\varphi_0)}{2}\right]$$

$$\times\int_{\varphi_0}^{\infty}d\varphi\,F(\varphi)\sin\left[\frac{ck_z(\varphi)}{2}\right]e^{-(\varphi-\varphi_0)/\omega_c\tau} \quad (5)$$

up to a constant of proportionality.

Performing the integration over k_z^0, we arrive at

$$\sigma_{zz} = \frac{2\pi}{c}\times\frac{m^*\cos(\theta)}{\omega_c}\int_0^{2\pi}d\varphi_0\,F(\varphi_0)\int_{\varphi_0}^{\infty}d\varphi\,F(\varphi)$$

$$\times\cos\left(-G(\varphi)+\frac{c}{2}\sum_{j=1}^{8}n_j(\varphi)\Delta k_z^{(j)}+G(\varphi_0)\right)$$

$$\times e^{-(\varphi-\varphi_0)/\omega_c\tau}, \quad (6)$$

where we define $G(\varphi) \equiv \frac{c}{2}\times k_F^{\parallel}(\varphi)\tan(\theta)\cos(\varphi-\phi)$.

We neglect the constant prefactor and use $\cos(x) = \text{Re}[e^{ix}]$ to write

$$\sigma_{zz} = \frac{m^*\cos(\theta)}{\omega_c}\text{Re}\Bigg[\int_0^{2\pi}d\varphi_0\,F(\varphi_0)\int_{\varphi_0}^{\infty}d\varphi\,F(\varphi)$$

$$\times e^{i[G(\varphi)-G(\varphi_0)]}e^{-(\varphi-\varphi_0)/\omega_c\tau}e^{\frac{-ic}{2}\sum_{j=1}^{8}n_j(\varphi)\Delta k_z^{(j)}}\Bigg]. \quad (7)$$

Note that the value of the integrand changes whenever the quasiparticle undergoes Bragg diffraction, due to the term $\sum n_j(\varphi)\Delta k_z^{(j)}$. In order to evaluate this integral, we must be able to account for all possible trajectories of each quasiparticle. Falicov and Sievert developed a method to handle such integrals when calculating in-plane conductivity [37], and recently Nowojewski *et al.* adapted their method to be used for AMRO [31].

Following the methods of Ref. [31], we separately consider the motion of quasiparticles starting in the eight different segments of the Fermi surface, then sum their contributions to the conductivity. To do so, we rewrite the above integral in a vectorized form:

$$\sigma_{zz} = \frac{m^*\cos(\theta)}{\omega_c}\times\text{Re}\{\boldsymbol{\lambda}_{\varphi_0}\cdot[\boldsymbol{\lambda}_{\text{init}}+\boldsymbol{\Gamma}(\boldsymbol{I}-\boldsymbol{\Gamma})^{-1}\boldsymbol{\lambda}_{\varphi}]\}. \quad (8)$$

In this equation, the dot product with $\boldsymbol{\lambda}_{\varphi_0}$ sums up all the possible initial positions of the quasiparticle, $\boldsymbol{\lambda}_{\text{init}}$ describes the initial motion of the quasiparticle up to an MB junction, and $\boldsymbol{\lambda}_{\varphi}$ describes the contribution to conductivity when the quasiparticle is between MB junctions. For our system, each vector has eight elements; the jth element of each vector is defined as follows:

$$\boldsymbol{\lambda}_{\varphi_0}[j] \equiv e^{-M_j/\omega_c\tau}\int_{M_j}^{M_{j+1}}d\varphi_0\,F(\varphi_0)e^{\varphi_0/\omega_c\tau}e^{-iG(\varphi_0)}$$

$$\boldsymbol{\lambda}_{\varphi}[j] \equiv e^{M_j/\omega_c\tau}\int_{M_j}^{M_{j+1}}d\varphi\,F(\varphi)e^{-\varphi/\omega_c\tau}e^{iG(\varphi)} \quad (9)$$

$$\boldsymbol{\lambda}_{\text{init}}[j] \equiv e^{M_j/\omega_c\tau}\int_{\varphi_0}^{M_{j+1}}d\varphi\,F(\varphi)e^{-\varphi/\omega_c\tau}e^{iG(\varphi)},$$

where

$$M \equiv \frac{\pi}{4} - \xi + \left[0, 2\xi, \frac{\pi}{2}, \frac{\pi}{2} + 2\xi, \pi, \pi + 2\xi, \frac{3\pi}{2}, \frac{3\pi}{2} + 2\xi, 2\pi \right] \tag{10}$$

is a vector giving the azimuthal position of each MB junction and the angle ξ is defined in Fig. 1(d).

The matrix $\mathbf{\Gamma}$ accounts for the connections between orbit segments, as well as the exponential damping of the integrand upon traversing a segment of Fermi surface. For our system, it is an 8×8 matrix:

$$\mathbf{\Gamma} \equiv \begin{pmatrix} 0 & ap & 0 & 0 & aqe^{-\frac{i}{2}\Delta k_z^{(2)}} & 0 & 0 & 0 \\ 0 & 0 & bp & 0 & 0 & 0 & 0 & bqe^{-\frac{i}{2}\Delta k_z^{(3)}} \\ 0 & 0 & 0 & ap & 0 & 0 & aqe^{-\frac{i}{2}\Delta k_z^{(4)}} & 0 \\ 0 & bqe^{-\frac{i}{2}\Delta k_z^{(5)}} & 0 & 0 & bp & 0 & 0 & 0 \\ aqe^{-\frac{i}{2}\Delta k_z^{(6)}} & 0 & 0 & 0 & 0 & ap & 0 & 0 \\ 0 & 0 & 0 & bqe^{-\frac{i}{2}\Delta k_z^{(7)}} & 0 & 0 & bp & 0 \\ 0 & 0 & aqe^{-\frac{i}{2}\Delta k_z^{(8)}} & 0 & 0 & 0 & 0 & ap \\ bp & 0 & 0 & 0 & 0 & bqe^{-\frac{i}{2}\Delta k_z^{(1)}} & 0 & 0 \end{pmatrix},$$

where $q = 1 - p$ and we have defined $a \equiv e^{-2\xi/\omega_c\tau}$ and $b \equiv e^{-(\pi/2 - 2\xi)/\omega_c\tau}$. See Appendix A for an explanation of the elements of $\mathbf{\Gamma}$.

As a simplification, we have assumed that the gaps that open in the Fermi surface upon reconstruction are of a negligible length in k space: we take the MB junction that ends one section of the Fermi surface to be in the same position as the MB junction that begins the next section.

With σ_{zz} in this vectorized form, we can quickly calculate numerical values for the conductivity with varying θ and ϕ.

III. APPLICATION TO A CUPRATE SUPERCONDUCTOR

We are now in a position to apply this model to a real system. We focus on $Tl_2Ba_2CuO_{6+\delta}$, since this is the cuprate that has been studied the most with AMRO [21,27,36,38]. As described by Hussey *et al.* [21], the Fermi surface of $Tl_2Ba_2CuO_{6+\delta}$ can be parameterized by $k_F^{\parallel}(\varphi) \equiv k_{00} + k_{40}\cos(4\varphi)$ and $F(\varphi) \equiv k_{21}\sin(2\varphi) + k_{61}\sin(6\varphi) + k_{101}\sin(10\varphi)$. The coefficients k_{mn} label an expansion of the Fermi surface in cylindrical harmonics appropriate for the space group symmetry of this material [36].

The AMRO of an unreconstructed Fermi surface can be produced by setting $B_0 = 0$, as shown in Figs. 3(a)–3(d) for two convenient values of $\omega_0\tau$. Note that $\omega_0\tau = 0.5$ reproduces the experimental AMRO observed by Hussey *et al.* at 4.2 K [21]. The AMRO for a system with (π,π) antiferromagnetic order is shown in Figs. 3(e)–3(h). This shows many qualitative differences with the unreconstructed state. The peak at $\theta = 0$ is strongly suppressed in the reconstructed Fermi surface. In addition, there are more Yamaji angles (peaks in the AMRO) for low polar angles θ in the unreconstructed state than the reconstructed state.

The evolution of the AMRO as we go from $B_0/B \approx 0$ to $B_0/B = 10$ for $\omega_0\tau = 0.5$ bears a striking resemblance to the evolution of the AMRO in $Tl_2Ba_2CuO_{6+\delta}$ with increasing temperature, most notably the disappearance of the hump at $\theta = 0$ [27,39]. This seems surprising, given that $Tl_2Ba_2CuO_{6+\delta}$ is not known to exhibit any static antiferromagnetic order,

though it has been shown to have strong antiferromagnetic fluctuations [40].

We explore the possibility that our AMRO calculations can capture some of the physics of $Tl_2Ba_2CuO_{6+\delta}$. Using the form of σ_{zz} above, we have produced simulations of out-of-plane resistivity as a function of angle using existing data for a sample with $T_c = 15$ K reported in Ref. [38]. The low-temperature (4.2 K) AMRO of $Tl_2Ba_2CuO_{6+\delta}$ is well fit by a simple model with no antiferromagnetic order ($B_0 = 0$), and using this data the functions $k_F^{\parallel}(\varphi)$ and $F(\varphi)$ that describe the Fermi surface can be fully determined in good agreement with previous work [21,27,36,38]. See Appendix D for more information on our determination of these parameters. We used geometric methods to solve for ξ and $\Delta k_z^{(j)}$ in this system, as explained in Appendixes B and C, respectively. To study the temperature-dependent AMRO above 4.2 K, we allowed only two free parameters: $\omega_0\tau$ and B_0. Note that in contrast to Ref. [38], $\omega_0\tau$ is fixed to be *isotropic* with azimuthal angle φ. We ran simulations across a large range of parameter space and used a least-squares fitting approach to determine the values of $\omega_0\tau$ and B_0 at each temperature. Our best fit to the data is shown in Fig. 4, showing excellent quantitative agreement with the AMRO of $Tl_2Ba_2CuO_{6+\delta}$. The temperature dependence of $\omega_0\tau$ and of B_0 as determined from the fits to data are shown in Fig. 5.

As can be seen in Fig. 3, more features are apparent in the AMRO when $\omega_0\tau$ is higher, making it easier to distinguish the effects of changing B_0. If $\omega_0\tau$ is decreased (by lowering magnetic fields, raising temperatures, or lowering sample quality), each quasiparticle will traverse less of the Fermi surface before it scatters. As illustrated in Fig. 6 of Ref. [41], this causes the amplitude of AMRO to be reduced, which makes an accurate determination of B_0 more difficult. Thus the error of our fitting parameters is greater at higher temperatures. Indeed, Ref. [38] includes AMRO data taken at 90 and 110 K, but we were not able to accurately determine B_0 at those elevated temperatures.

While Ref. [38] reproduced the observed AMRO using an anisotropic scattering rate, we find good quantitative agreement with the data using a magnetic breakdown model
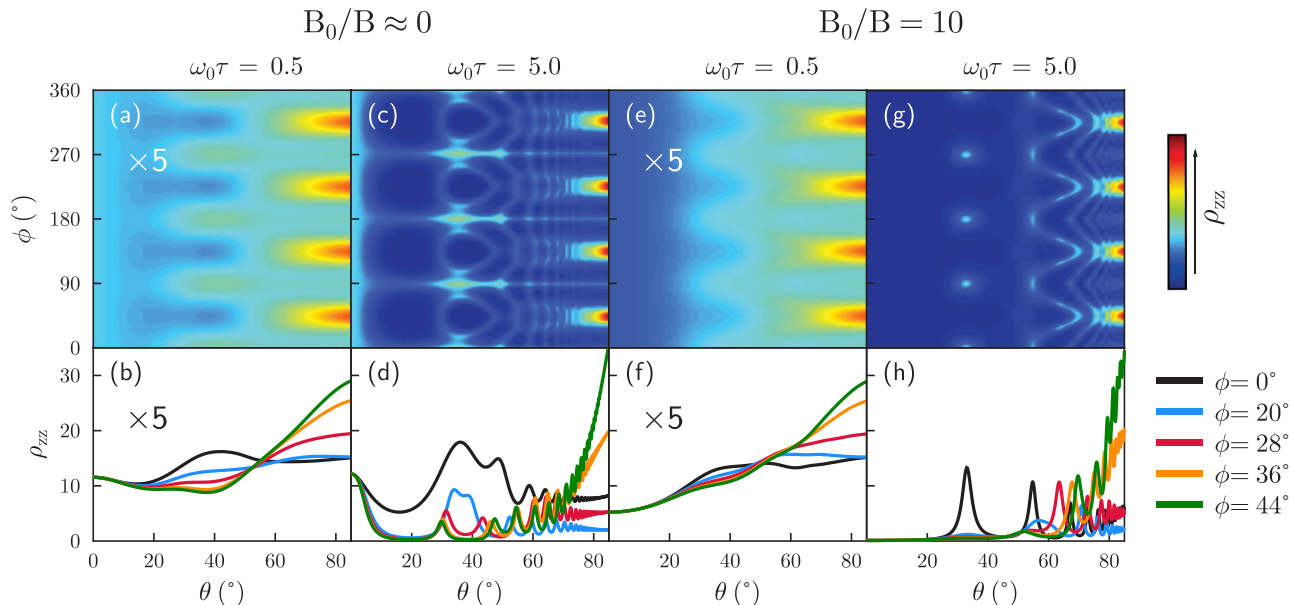
FIG. 3. (Color online) Calculated dimensionless resistivity of $Tl_2Ba_2CuO_{6+\delta}$ as a function of the orientation of applied magnetic field for different values of B_0/B and $\omega_0\tau$. We plot resistivity in units of $\pi^4\hbar^4\omega_0/m_0^*c(aet_\perp k_{21})^2$ so that it is dimensionless. The resistivity in plots (a, b) and (e, f) is scaled up by a factor of 5 for visual clarity. (a, c, e, g) Interlayer resistivity as a function of both θ and ϕ. (b, d, f, h) Interlayer resistivity as a function of θ for select values of ϕ; these azimuthal angles were chosen to facilitate comparison to Ref. [21].

with an isotropic scattering rate. Bragg scattering at a MB junction mimics the effect of an anisotropic scattering rate on an unreconstructed Fermi surface. However, importantly, the magnetic breakdown model connects specific parts of the Fermi surface in a single (Bragg) scattering event, while

the anisotropic scattering rate is a broad modulation of the quasiparticle lifetime about the Fermi surface. The similarity of the two models in reproducing the AMRO suggests that the apparent anisotropic scattering rate is a symptom of antiferromagnetism, perhaps involving short-range fluctuations. This could explain the different temperature dependence of the isotropic and anisotropic components of the scattering rate observed in Ref. [27].
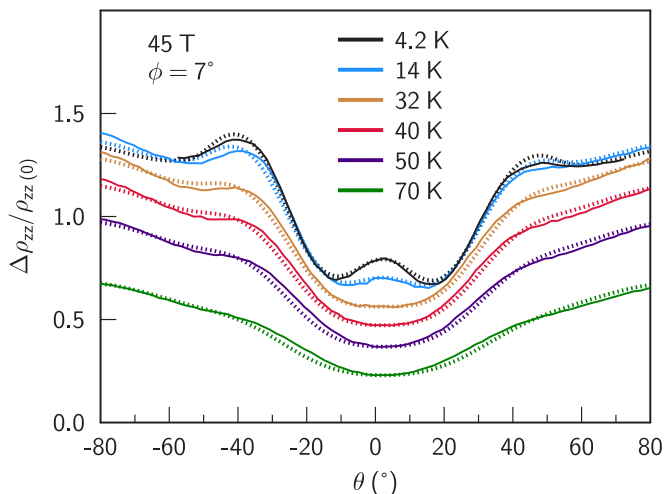
IV. DISCUSSION

The behavior of $\omega_0\tau$ in Fig. 5(a) indicates a natural (approximately linear) increase in the scattering rate with temperature. The evolution of B_0 may reflect deeper physics. As shown in Fig. 5(b), B_0 increases quickly with temperature, peaking at around 45 K. The parameter B_0 is a measure of

FIG. 4. (Color online) Temperature dependence of the interlayer AMRO of overdoped $Tl_2Ba_2CuO_{6+\delta}$ ($T_c = 15$ K) at a fixed field of 45 T and a fixed azimuthal direction of $\phi = 7°$. The solid lines are c-axis magnetoresistivity data, taken from French *et al.* [38]. These data have been normalized to the zero-field resistivity of the sample at each temperature. The dashed lines are simulations of AMRO for $Tl_2Ba_2CuO_{6+\delta}$ under antiferromagnetic order, calculated as described in the text. The simulations have been scaled to match the data at $\theta = 0°$ for each temperature. When producing these simulations, all the parameters related to Fermi surface geometry were fixed and the only parameters allowed to vary with temperature were $\omega_0\tau$ and B_0.
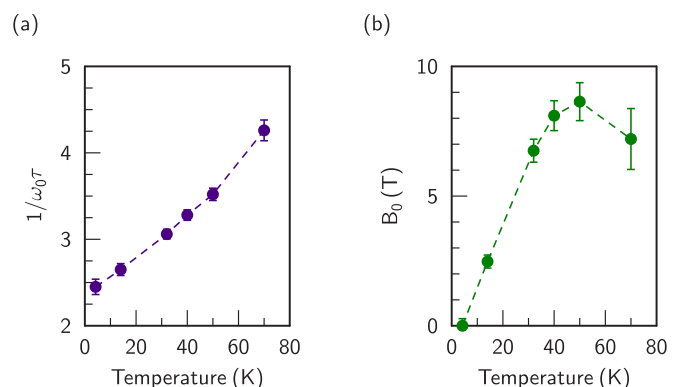

FIG. 5. (Color online) Temperature dependence of (a) $1/\omega_0\tau$ and (b) B_0 extracted from fits to data. Error bars are standard errors extracted from the covariance matrix of the least-squares fitting at each temperature (see Appendix D).

the probability of Bragg scattering. For a static reconstructed Fermi surface, this is related to the separation between reconstructed sections, which is in turn proportional to the band gap [26]. Therefore under static reconstruction we would expect B_0 to be largest at 0 K and decrease weakly with increasing temperature [26,42]. In the presence of antiferromagnetic fluctuations, similar scattering events might still occur at points where the reconstructed Brillouin zone intersects the Fermi surface. In this case, B_0 will play two roles: in addition to parameterizing the separation between sections of Fermi surface, it also reflects the probability of Bragg scattering within the time/length scale of the fluctuations [43]. Note that in the overdoped cuprates, there is a known crossover in the transport from Fermi-liquid–like to non-Fermi-liquid–like behavior with increasing temperature that is thought to be associated with critical fluctuations [44]. In this picture, the increase of B_0 with temperature seen in Fig. 5(b) can be interpreted as an increase in antiferromagnetic fluctuations. As the temperature rises and antiferromagnetic fluctuations grow, quasiparticles have a nonzero chance of undergoing Bragg diffraction when they reach MB junctions, so B_0 attains a nonzero value. At still higher temperatures, the antiferromagnetic correlation time is so short that the effect of Bragg scattering decreases, resulting in a decrease in B_0. The evolution of B_0 looks strikingly similar to the evolution of the imaginary part of the dynamic susceptibility Imχ (which is a measure of the magnetic scattering) seen in a number of neutron experiments in cuprate superconductors; consider, for example, Fig. 10 of Ref. [45]. We therefore suggest that the temperature dependence of B_0 in Fig. 5(b) reflects the effect of antiferromagnetic fluctuations on the magnetotransport.

For the above to be plausible, the antiferromagnetic fluctuations of the system should be on a long enough time scale to affect the quasiparticles' motion about the Fermi surface: the time scale of an antiferromagnetic fluctuation should be longer than the time it takes for a quasiparticle to traverse a section of Fermi surface from one MB junction to the next. The antiferromagnetic fluctuations in $La_{2-x}Sr_xCuO_4$ near optimal doping have a frequency that is roughly linearly proportional to temperature [46]. Taking this as a guide, we estimate that the time scale of an antiferromagnetic fluctuation will be of the order $\tau_{AF} \sim \frac{\hbar}{k_B T}$. Meanwhile, the time for a quasiparticle to cross the smallest section of Fermi surface between two MB junctions is given by $\tau_{QP} \sim \frac{1}{\omega_c} \frac{\pi/2 - 2\xi}{2\pi}$. Therefore our condition $\tau_{AF} > \tau_{QP}$ is equivalent to

$$\hbar\omega_c > \frac{\pi/2 - 2\xi}{2\pi} k_B T. \tag{11}$$

For this system the requirement is approximately

$$\frac{\omega_c}{T} > 3.6 \times 10^9 \text{ s}^{-1} \text{ K}^{-1}. \tag{12}$$

Using $m^* \approx 5 m_e$ [47], we find $\omega_c \approx 1.6 \times 10^{12}$ s^{-1} at 45 T and with $\theta = 0°$. Therefore antiferromagnetic fluctuations could be expected to affect quasiparticle motion up to $T \approx 400$ K, much higher than the temperature regime studied in this paper.

The magnetic breakdown picture of the effect of antiferromagnetic fluctuations on AMRO could be substantially improved by including a more realistic model of the MB junctions in a fluctuating system that includes, for example, a distribution of ordering wave vectors about (π,π) [16]. Nevertheless,

this simple model captures many of the important features observed in the temperature-dependent AMRO without the need for a multicomponent scattering with a different nodal and antinodal temperature dependence [27,36,38]. This model may also prove useful for understanding further transport properties of $Tl_2Ba_2CuO_{6+\delta}$ (see Appendix E). Moreover, our results suggest there is a potential link between B_0 and the dynamic susceptibility Imχ. If this connection can find a sound theoretical basis, it may open the way for the use of AMRO as an experimental probe of magnetic scattering.

V. CONCLUSION

We have developed a simple and computationally inexpensive numerical method to calculate AMRO in layered two-dimensional materials with (π,π) antiferromagnetic order. This model can be applied to both hole- and electron-doped cuprates with an appropriately adjusted Fermi surface parametrization for direct comparison with experimental data. In addition, our numerical method can easily be applied to states other than (π,π) ordering, such as the charge-ordered states recently proposed in underdoped $YBa_2Cu_3O_{6+\delta}$ [6,17,18,20] and $HgBa_2CuO_{6+\delta}$ [48]. We have shown that an antiferromagnetic Fermi surface reconstruction with a temperature-dependent magnetic breakdown field can fit the AMRO of $Tl_2Ba_2CuO_{6+\delta}$, an overdoped compound with no static order. The agreement between our fits and the AMRO data suggests that the features attributed to scattering anisotropy in these systems [27,36,38] may in fact be due to fluctuations of a (π,π) ordering such as antiferromagnetism, and indeed that the MB field B_0 can potentially be used as an experimental measure of such fluctuations. This would make AMRO a good complement to scattering probes of fluctuations, such as neutron scattering and resonant inelastic x-ray scattering. We propose that future AMRO experiments at higher magnetic fields and in materials where Imχ has been determined independently by neutron scattering would provide an instructive comparison to test the validity of this connection.

APPENDIX A: GENERAL METHOD FOR CALCULATING CONDUCTIVITY WITH MAGNETIC BREAKDOWN

In this Appendix we describe a step-by-step method to calculate σ_{zz} in a Q2D material with magnetic breakdown effects.

(1) Consider the full, warped-cylindrical Fermi surface that would exist were the Fermi surface not reconstructed. Using existing data or theories, determine a likely form of this Fermi surface as a function of k_z and φ. This may be exactly fixed or it may contain free parameters to be fitted.

(2) Use the Fermi surface to determine $v_\alpha(\boldsymbol{k},\varphi)$ and $v_\beta(\boldsymbol{k},\varphi)$ for the element $\sigma_{\alpha\beta}$ in question. Note that v_x and v_y are not simply proportional to k_x and k_y for a noncircular Fermi surface; see the section on in-plane transport below.

(3) Insert these velocities into the Boltzmann transport equation as given in Eq. (1) of the main text. Wherever k_z appears in the integrand, replace it with the following function of φ:

$$k_z(\varphi) = k_z^0 - k_F^{\|}(\varphi)\tan(\theta)\cos(\varphi - \phi) + \sum_j n_j(\varphi)\Delta k_z^{(j)}.$$
(A1)

(4) Replace the integral over k_B with an integral over k_z^0 multiplied by $\cos(\theta)$, and perform the integration over k_z^0. At this point, it should be possible to write the Boltzmann transport equation in the form

$$\sigma_{\alpha\beta} = C_1 \int_0^{2\pi} d\varphi_0 \; f_1(\varphi_0) \int_{\varphi_0}^\infty d\varphi \; f_2(\varphi) e^{C_2 \sum_j n_j(\varphi)\Delta k_z^{(j)}}, \quad \text{(A2)}$$

where f_1 and f_2 are functions, and C_1 and C_2 are constants. Note that C_2 will be zero if $\beta = x$ or y.

(5) Determine geometrically where the Fermi surface will intersect the (reconstructed) Brillouin zone. These points are the magnetic breakdown junctions. Write a vector, $\boldsymbol{M}$, giving the azimuthal position of each junction and ending at the location of the first junction plus 2π. Be sure that the definition of $\varphi = 0$ for this vector is consistent with the definition of $\varphi = 0$ for the Fermi surface warping. The length of $\boldsymbol{M}$ will be $n + 1$, where n is the number of MB junctions around the Fermi surface.

(6) Define three vectors of length n as follows:

$$\boldsymbol{\lambda_{\varphi_0}}[j] \equiv e^{-\boldsymbol{M}_j/\omega_c\tau} \int_{\boldsymbol{M}_j}^{\boldsymbol{M}_{j+1}} d\varphi_0 \; f_1(\varphi_0)$$

$$\boldsymbol{\lambda_\varphi}[j] \equiv e^{\boldsymbol{M}_j/\omega_c\tau} \int_{\boldsymbol{M}_j}^{\boldsymbol{M}_{j+1}} d\varphi \; f_2(\varphi) \quad \text{(A3)}$$

$$\boldsymbol{\lambda}_{\text{init}}[j] \equiv e^{\boldsymbol{M}_j/\omega_c\tau} \int_{\varphi_0}^{\boldsymbol{M}_{j+1}} d\varphi \; f_2(\varphi).$$

(7) Define the $n \times n$ matrix $\boldsymbol{\Gamma}$. Each row (column) of $\boldsymbol{\Gamma}$ corresponds to a specific *section* of the Fermi surface between two MB junctions. The first row of $\boldsymbol{\Gamma}$ corresponds to the section between the first and second MB junctions, as defined in the vector $\boldsymbol{M}$; the second row corresponds to the section between the second and third MB junctions; and so on. The elements in each row are as follows:

$$\boldsymbol{\Gamma}_{ij} = \begin{cases} 0 & \text{if section } i \text{ has no connection to section } j \\ a_i\, p & \begin{array}{l}\text{if section } i \text{ is connected to section } j \text{ through magnetic breakdown} \\ \text{(i.e., the quasiparticle on section } i \text{ goes to section } j \text{ by following the} \\ \text{full cylindrical Fermi surface)} \end{array} \\ a_i(1-p)e^{C_2\Delta k_z^{(i+1)\to j}} & \begin{array}{l}\text{if section } i \text{ is connected to section } j \text{ through Bragg diffraction} \\ \text{(i.e., the quasiparticle on section } i \text{ goes to section } j \text{ by following the} \\ \text{reconstructed Fermi surface),}\end{array} \end{cases} \quad \text{(A4)}$$

where $p = e^{-B_0/B\cos(\theta)}$ is the magnetic breakdown probability, and $a_i \equiv e^{-(M_{i+1}-M_i)/\omega_c\tau}$. The term a_i accounts for the damping of our integrand as the quasiparticle traverses the ith section of the Fermi surface. Note the term $\Delta k_z^{(i+1)\to j}$: after traversing the ith section of the Fermi surface, the quasiparticle would Bragg diffract from the $(i + 1)$th magnetic breakdown junction. The terms $\Delta k_z^{(i+1)\to j}$ can be calculated as described in Appendix C below.

(8) Using the objects defined above, calculate the conductivity for a given direction of the applied field:

$$\sigma_{\alpha\beta}(\theta,\phi) = C_1 \times \text{Re}\{\boldsymbol{\lambda_{\varphi_0}} \cdot [\boldsymbol{\lambda}_{\text{init}} + \boldsymbol{\Gamma}(\boldsymbol{I} - \boldsymbol{\Gamma})^{-1}\boldsymbol{\lambda_\varphi}]\}. \quad \text{(A5)}$$

Note that the dot product $\boldsymbol{\lambda_{\varphi_0}} \cdot \boldsymbol{\lambda}_{\text{init}}$ yields a double integral over φ_0 and φ and must be evaluated as such.

APPENDIX B: CALCULATING ξ

The angle ξ is defined as shown in Fig. 6. If the Fermi surface were completely cylindrical, it would obey

$$\cos(\xi) = \frac{\pi}{a_{\text{AF}}k_F},$$

where a_{AF} is the in-plane lattice parameter of the antiferromagnetically ordered system and k_F is the Fermi momentum. We may neglect the interlayer warping of the Fermi surface, which is relatively weak, but not the in-plane warping. Therefore we have the relation

$$\cos(\xi) = \frac{\pi}{a_{AF}[k_{00} + k_{40}\cos(4\xi)]},$$

which can be solved self-consistently for ξ. We know that $a_{\text{AF}} = \sqrt{2}a$. We use $a = 0.3866$ nm, as given by Analytis *et al.* [36]. We use $k_{00} = 7.30$ nm^{-1} and $k_{40} = -0.234$ nm^{-1}. These are the values found by French *et al.* from fitting their
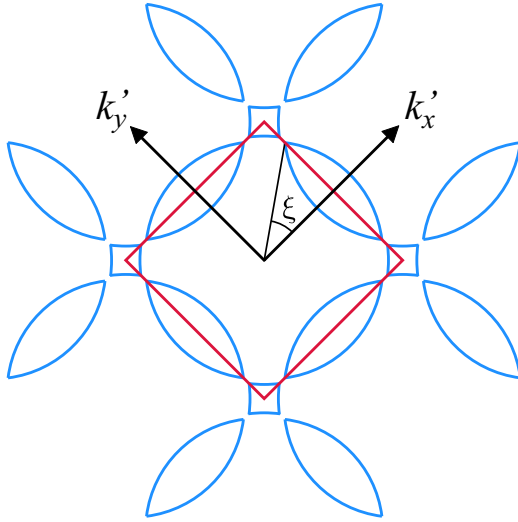
FIG. 6. (Color online) The angle ξ is defined with respect to the reconstructed Fermi surface of $Tl_2Ba_2CuO_{6+\delta}$. The Fermi surface is shown in the repeated zone scheme, with the reconstructed Brillouin zone overlaid.

4.2-K AMRO data [38] and they are consistent with the results of our fits (see above). Using these values, we find $\xi \approx 40.18°$. Due to uncertainty in the Fermi surface fits, we cannot calculate ξ with accuracy beyond two significant digits. We therefore round to $\xi = 40°$ for use in our fits to high-temperature data.

APPENDIX C: CALCULATING $\Delta k_z^{(j)}$

As stated in the main text, we can define a vector giving the azimuthal position of each magnetic breakdown (MB) junction as follows:

$$\boldsymbol{M} \equiv \frac{\pi}{4} - \xi + \left[0, \ 2\xi, \ \frac{\pi}{2}, \ \frac{\pi}{2} + 2\xi, \ \pi, \pi \right.$$
$$\left. + 2\xi, \ \frac{3\pi}{2}, \ \frac{3\pi}{2} + 2\xi, \ 2\pi \right]. \quad \text{(C1)}$$

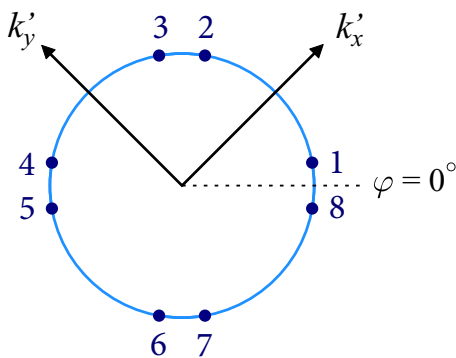The position of these MB junctions on the (unreconstructed) Fermi surface is shown in Fig. 7.

FIG. 7. (Color online) Position of the eight magnetic breakdown junctions on the Fermi surface of $Tl_2Ba_2CuO_{6+\delta}$ under (π,π) order. The reciprocal space axes shown correspond to the reconstructed Brillouin zone.

To find the values of $\Delta k_z^{(j)}$, we must know where a quasiparticle goes when it experiences Bragg diffraction at a given MB junction. To determine this, we need only see which MB junctions are connected by reciprocal lattice vectors of the reconstructed Brillouin zone. They are the following: $1 \leftrightarrow 6$, $2 \leftrightarrow 5$, $3 \leftrightarrow 8$, $4 \leftrightarrow 7$.

An easy way to understand these pairings is to examine the small Fermi surface orbits that the quasiparticle will follows if it Bragg diffracts at every junction (see Fig. 8).

As stated in the main text, a quasiparticle undergoing Bragg diffraction in this system will have $k_z^{(i)} = k_z^{(f)}$. We neglect the weak interlayer warping of the system; then for a quasiparticle on a particular slice of the Fermi surface, we can write

$$k_z(\varphi) = k_z^0 - k_F^{\parallel}(\varphi) \tan(\theta) \cos(\varphi - \phi). \quad \text{(C2)}$$

This leads to the condition

$$k_z^{0(i)} - k_F^{\parallel}(\varphi_i) \tan(\theta) \cos(\varphi_i - \phi)$$
$$= k_z^{0(f)} - k_F^{\parallel}(\varphi_f) \tan(\theta) \cos(\varphi_f - \phi), \quad \text{(C3)}$$

and therefore

$$\Delta k_z^{(i \to f)} = k_z^{0(f)} - k_z^{0(i)}$$
$$= \tan(\theta)[k_F^{\parallel}(\varphi_f) \cos(\varphi_f - \phi) - k_F^{\parallel}(\varphi_i) \cos(\varphi_i - \phi)]. \quad \text{(C4)}$$

Since φ_i and φ_f are given by the vector $\boldsymbol{M}$, we now have everything we need to solve for $\Delta k_z^{(i \to f)}$ for each possible Bragg diffraction. For example, if a quasiparticle is going from MB junction 1 to MB junction 6 we have $\varphi_i = \frac{\pi}{4} - \xi$ and $\varphi_f = \frac{\pi}{4} - \xi + \pi + 2\xi = \frac{5\pi}{4} + \xi$. We can use these to solve for $\Delta k_z^{(1 \to 6)}$, which we denote as $\Delta k_z^{(1)}$ for the sake of brevity.

APPENDIX D: PARAMETER FITTING AND ERROR BARS

We would expect the parameters k_{mn} to be constant with temperature, as they describe the Fermi surface geometry. Therefore we can fit these parameters from our 4.2-K data, since we do not expect reconstruction and magnetic breakdown to occur at this temperature. From band structure calculations [49] and from previous AMRO studies [21], we expect this material to have no c-axis dispersion along the zone diagonals, as well as along the lines $k_x = \pi$ and $k_y = \pi$. In order for this to be realized, it must be the case that $1 - k_{61}/k_{21} + k_{101}/k_{21} = 0$ [50].

We simulated conductivity for a wide swath of parameter space and used a least-squares fitting to data to arrive at the following: $k_{00} = 7.34 \text{ nm}^{-1}$, $k_{40} = -0.25 \text{ nm}^{-1}$, $k_{61}/k_{21} = 0.69$ (and therefore $k_{101}/k_{21} = -0.31$) [51].

Simultaneously with fitting the Fermi surface geometry, we used the 4.2-K data to fit for the misalignment of the crystal with respect to the magnetic field; see Analytis *et al.* for details on the significance and calculation of this misalignment [36]. We obtained the best fits to data from $\Phi_{asym} = -0.6°$, $\Theta_{asym}^x = -2.5°$, and $\Theta_{asym}^y = -2.8°$.

Once we have fit these parameters at 4.2 K, the only parameters free to fit for the data as a function of temperature are
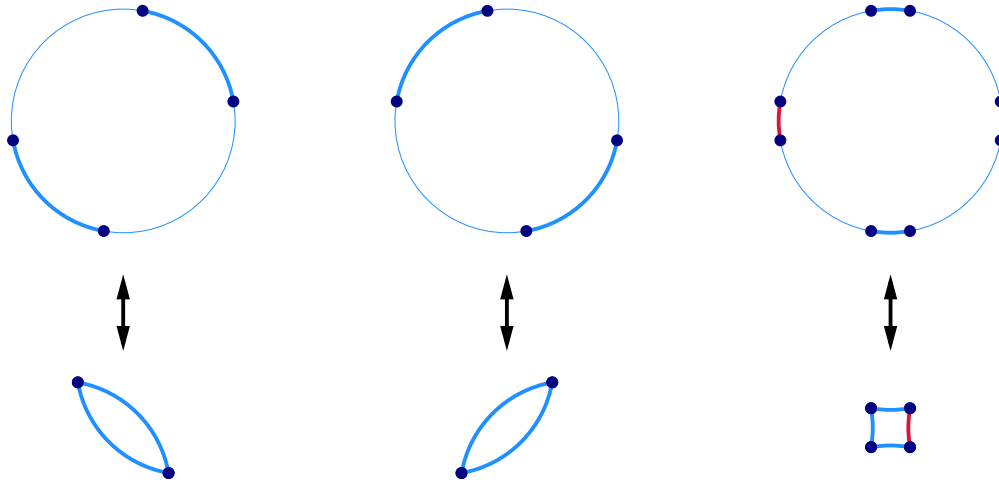
FIG. 8. (Color online) Three small Fermi surface pockets are formed when the Fermi surface of $Tl_2Ba_2CuO_{6+\delta}$ is reconstructed under (π,π) order.

B_0 and $1/\omega_0\tau$. For each temperature we simulated conductivity across a broad range of B_0 and $1/\omega_0\tau$ and used a least-squares fitting to arrive at the following values for the best fits to data:

T (K)	B_0 (T)	$1/\omega_0\tau$
4.2	0[a]	2.50
14	2.5	2.65
32	6.8	3.06
40	8.1	3.28
50	8.6	3.52
70	7.2	4.26

[a]We assumed $B_0 = 0$ at 4.2 K in order to perform our fits for Fermi surface geometry and alignment.

The error bars shown on B_0 and $1/\omega_0\tau$ in the main text are the standard error of those parameters. At each temperature, the values of B_0 and $1/\omega_0\tau$ that give the best fit to data are those for which the sum of squared error (SSE) between data and simulation is minimized. We can fit the SSE to a functional form in terms of B_0 and $1/\omega_0\tau$ about that minimum. We use this functional form to approximate the Hessian matrix for these two parameters, the inverse of which is the covariance matrix, $\boldsymbol{C}$. The standard error for each parameter is then simply given by $\sqrt{C_{ii}/(N-2)}$, where N is the number of data points we used for the fitting at that temperature (and two is the number of parameters we fit). Which diagonal element of $\boldsymbol{C}$ corresponds to each parameter depends on how we construct the Hessian matrix.

APPENDIX E: IN-PLANE TRANSPORT SIMULATIONS

In addition to calculating σ_{zz}, we can use the same methods as detailed above to calculate the in-plane components of the conductivity tensor [52]. Neglecting the weak interlayer warping of our system, we find $v_x(\varphi) = \frac{\hbar}{m^*} k_F^{\parallel}(\varphi) \cos(\varphi - \gamma)$ and $v_y(\varphi) = \frac{\hbar}{m^*} k_F^{\parallel}(\varphi) \sin(\varphi - \gamma)$. Here γ is the angle between v_F and a vector pointing radially outward towards the Fermi

surface, and it is given by

$$\gamma(\varphi) = \tan^{-1}\left[\frac{\partial}{\partial\varphi}[\log k_F(\varphi)]\right], \quad (E1)$$

as described in Ref. [53]. The procedure is then nearly identical to that for σ_{zz}, though slightly simplified by the fact that the $\Delta k_z^{(j)}$ terms are not involved in the in-plane calculations. We can calculate in-plane conductivity exactly, whereas we can only calculate σ_{zz} up to a constant of proportionality since we do not know the value of $t_\perp$.

Rather than calculating the in-plane transport terms and fitting them to experimental data, we want to see what predictions we can make for in-plane transport based on our analysis of the interlayer transport. We fit the points from Fig. 5 in the main text to analytical functions: a second-order polynomial in temperature for $1/\omega_0\tau$, and a function of the form $\frac{c_1}{T}e^{-c_2/T}$ for B_0, as we expect that at higher temperatures B_0 must decrease due to weakening antiferromagnetic correlations.

Using these analytical functions of our temperature-dependent parameters, we are able to calculate the in-plane transport of $Tl_2Ba_2CuO_{6+\delta}$ at any temperature—though such calculations should be interpreted with care because we are extrapolating to higher temperatures using information that comes from 50 K and below. We can compare these calculations to data taken from comparable samples by Mackenzie *et al.* [54], as shown in Fig. 9. Note that the data presented in these figures come from a sample with T_c of 15 K, the same critical temperature as the sample whose AMRO data we have analyzed.

Our simulations of in-plane transport are qualitatively similar to experimental data, though they do not agree quantitatively, especially the Hall angle and Hall coefficient. It is important to note that in the magnetic breakdown model, where B_0/B plays an important role, we do not have Drude-like resistivity: ρ_{xy} is not directly proportional to the magnetic field. Therefore we would have to use Hall data taken at 45 T to truly make a meaningful comparison. We cannot simply lower the magnetic field strength in our calculations to match the field at which data was taken, as we only have information on B_0 for a 45-T field. It has been proposed that antiferromagnetism in
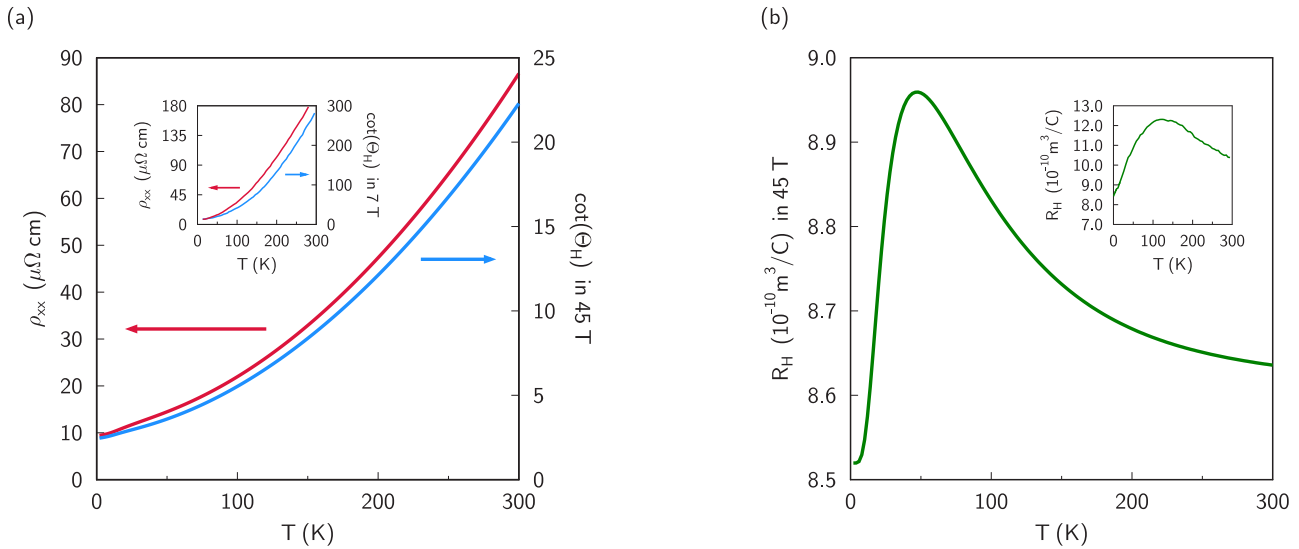
FIG. 9. (Color online) Simulations of in-plane transport for $Tl_2Ba_2CuO_{6+\delta}$ compared to experimental data taken from Ref. [54]. (a) Calculated values for the in-plane resistivity and for the cotangent of the Hall angle in a 45-T field plotted versus temperature (inset: data at 7 T). (b) Calculated values of the Hall coefficient as a function of temperature in a 45-T field (inset: data at unspecified field).

the cuprates is enhanced by an applied magnetic field [55,56] and therefore we cannot assume that the value of B_0 at lower fields matches that at 45 T.

We show these results not because they definitively support or contradict the magnetic breakdown model, but merely in the spirit of sharing the results of our explorations. Given that we do not know the dependence of B_0 on B, it seems unlikely that such in-plane calculations can yield strong evidence for or against the suggested model unless new in-plane transport data are taken at 45 T.

[1] J. L. Tallon and J. W. Loram, Physica C **349**, 53 (2001).

[2] A. Shekhter, B. J. Ramshaw, R. Liang, W. N. Hardy, D. A. Bonn, F. F. Balakirev, R. D. McDonald, J. B. Betts, S. C. Riggs, and A. Migliori, Nature (London) **498**, 75 (2013).

[3] J. Xia, E. Schemm, G. Deutscher, S. A. Kivelson, D. A. Bonn, W. N. Hardy, R. Liang, W. Siemons, G. Koster, M. M. Fejer, and A. Kapitulnik, Phys. Rev. Lett. **100**, 127002 (2008).

[4] R.-H. He, M. Hashimoto, H. Karapetyan, J. D. Koralek, J. P. Hinton, J. P. Testaud, V. Nathan, Y. Yoshida, H. Yao, K. Tanaka, W. Meevasana, R. G. Moore, D. H. Lu, S.-K. Mo, M. Ishikado, H. Eisaki, Z. Hussain, T. P. Devereaux, S. A. Kivelson, J. Orenstein, A. Kapitulnik, and Z.-X. Shen, Science **331**, 1579 (2011).

[5] K. McElroy, D.-H. Lee, J. E. Hoffman, K. M. Lang, J. Lee, E. W. Hudson, H. Eisaki, S. Uchida, and J. C. Davis, Phys. Rev. Lett. **94**, 197005 (2005).

[6] E. H. d. S. Neto, P. Aynajian, A. Frano, R. Comin, E. Schierle, E. Weschke, A. Gyenis, J. Wen, J. Schneeloch, Z. Xu, S. Ono, G. Gu, M. L. Tacon, and A. Yazdani, Science **343**, 393 (2014).

[7] O. Cyr-Choinire, G. Grissonnanche, S. Badoux, J. Day, D. A. Bonn, W. N. Hardy, R. Liang, N. Doiron-Leyraud, and L. Taillefer, arXiv:1504.06972.

[8] S. Lederer, Y. Schattner, E. Berg, and S. A. Kivelson, Phys. Rev. Lett. **114**, 097001 (2015).

[9] P. Monthoux, D. Pines, and G. G. Lonzarich, Nature (London) **450**, 1177 (2007).

[10] S. Sachdev, M. A. Metlitski, and M. Punk, J. Phys.: Condens. Matter **24**, 294205 (2012).

[11] J. C. S. Davis and D.-H. Lee, Proc. Natl. Acad. Sci. USA **110**, 17623 (2013).

[12] N. Doiron-Leyraud, C. Proust, D. LeBoeuf, J. Levallois, J.-B. Bonnemaison, R. Liang, D. A. Bonn, W. N. Hardy, and L. Taillefer, Nature (London) **447**, 565 (2007).

[13] S. E. Sebastian, N. Harrison, R. Liang, D. A. Bonn, W. N. Hardy, C. H. Mielke, and G. G. Lonzarich, Phys. Rev. Lett. **108**, 196403 (2012).

[14] B. J. Ramshaw, S. E. Sebastian, R. D. McDonald, J. Day, B. S. Tan, Z. Zhu, J. B. Betts, R. Liang, D. A. Bonn, W. N. Hardy, and N. Harrison, Science **348**, 317 (2015).

[15] T. Helm, M. V. Kartsovnik, M. Bartkowiak, N. Bittner, M. Lambacher, A. Erb, J. Wosnitza, and R. Gross, Phys. Rev. Lett. **103**, 157002 (2009).

[16] N. Harrison, R. D. McDonald, and J. Singleton, Phys. Rev. Lett. **99**, 206406 (2007).

[17] T. Wu, H. Mayaffre, S. Krämer, M. Horvatić, C. Berthier, W. N. Hardy, R. Liang, D. A. Bonn, and M.-H. Julien, Nature (London) **477**, 191 (2011).

[18] T. Wu, H. Mayaffre, S. Krämer, M. Horvatić, C. Berthier, P. L. Kuhns, A. P. Reyes, R. Liang, W. N. Hardy, D. A. Bonn, and M.-H. Julien, Nat. Commun. **4**, 2113 (2013).

[19] T. P. Croft, C. Lester, M. S. Senn, A. Bombardi, and S. M. Hayden, Phys. Rev. B **89**, 224513 (2014).

[20] D. LeBoeuf, S. Krämer, W. N. Hardy, R. Liang, D. A. Bonn, and C. Proust, Nat. Phys. **9**, 79 (2013).

[21] N. E. Hussey, M. Abdel-Jawad, A. Carrington, A. P. Mackenzie, and L. Balicas, Nature (London) **425**, 814 (2003).

[22] M. V. Kartsovnik, Chem. Rev. **104**, 5737 (2004).

[23] A. G. Lebed, N. N. Bagmet, and M. J. Naughton, Phys. Rev. Lett. **93**, 157006 (2004).

[24] K. Yamaji, J. Phys. Soc. Jpn. **58**, 1520 (1989).

[25] P. A. Goddard, S. J. Blundell, J. Singleton, R. D. McDonald, A. Ardavan, A. Narduzzo, J. A. Schlueter, A. M. Kini, and T. Sasaki, Phys. Rev. B **69**, 174509 (2004).

[26] D. Shoenberg, in *Magnetic Oscillations in Metals* (Cambridge University Press, Cambridge, UK, 1984), pp. 331–368.

[27] M. Abdel-Jawad, M. P. Kennett, L. Balicas, A. Carrington, A. P. Mackenzie, R. H. McKenzie, and N. E. Hussey, Nat. Phys. **2**, 821 (2006).

[28] J. Kokalj, N. E. Hussey, and R. H. McKenzie, Phys. Rev. B **86**, 045132 (2012).

[29] L. Dell'Anna and W. Metzner, Phys. Rev. Lett. **98**, 136402 (2007).

[30] J. Chang, M. Månsson, S. Pailhès, T. Claesson, O. J. Lipscombe, S. M. Hayden, L. Patthey, O. Tjernberg, and J. Mesot, Nat. Commun. **4**, 2559 (2013).

[31] A. Nowojewski, P. A. Goddard, and S. J. Blundell, Phys. Rev. B **77**, 012402 (2008).

[32] Note that in two-dimensional material, the quasiparticle faces a larger k-space tunneling barrier when its orbit is tilted; we therefore write $p = e^{-B_0/B\cos(\theta)}$ so that B_0 itself has no angular dependence.

[33] J. M. Ziman, in *Principles of the Theory of Solids* (Cambridge University Press, Cambridge, UK, 1972), p. 301.

[34] We have defined $\varphi \equiv \varphi_0 + \varphi'$ to rewrite the bounds of integration as given by Ziman [33]. The slight difference between this form and that given by Ziman is then merely the difference of whether one considers the quasiparticle to be traveling clockwise or counterclockwise about the Fermi surface.

[35] R. Yagi, Ph.D. thesis, University of Tokyo, 1991.

[36] J. G. Analytis, M. Abdel-Jawad, L. Balicas, M. M. J. French, and N. E. Hussey, Phys. Rev. B **76**, 104523 (2007).

[37] L. M. Falicov and P. R. Sievert, Phys. Rev. **138**, A88 (1965).

[38] M. M. J. French, J. G. Analytis, A. Carrington, L. Balicas, and N. E. Hussey, New J. Phys. **11**, 055057 (2009).

[39] M. Abdel-Jawad, J. G. Analytis, L. Balicas, A. Carrington, J. P. H. Charmant, M. M. J. French, and N. E. Hussey, Phys. Rev. Lett. **99**, 107002 (2007).

[40] M. Le Tacon, M. Minola, D. C. Peets, M. Moretti Sala, S. Blanco-Canosa, V. Hinkov, R. Liang, D. A. Bonn, W. N. Hardy, C. T. Lin, T. Schmitt, L. Braicovich, G. Ghiringhelli, and B. Keimer, Phys. Rev. B **88**, 020501(R) (2013).

[41] P. D. Grigoriev, Phys. Rev. B **81**, 205122 (2010).

[42] J. Fenton and A. J. Schofield, Phys. Rev. Lett. **95**, 247201 (2005).

[43] The general form of the breakdown probability would be $p = 1 + g(T)(e^{-B_0/B\cos(\theta)} - 1)$, where $g(T)$ parameterizes the temperature-dependent strength of fluctuations. However, adding extra parameters in this way does not add any clarity to our interpretation of the AMRO data.

[44] N. E. Hussey, R. A. Cooper, X. Xu, Y. Wang, I. Mouzopoulou, B. Vignolle, and C. Proust, Philos. Trans. R. Soc. London A **369**, 1626 (2011).

[45] J. Rossat-Mignod, L. P. Regnault, C. Vettier, P. Bourges, P. Burlet, J. Bossy, J. Y. Henry, and G. Lapertot, Physica B **180**, 383 (1992).

[46] Y. Zha, V. Barzykin, and D. Pines, Phys. Rev. B **54**, 7561 (1996).

[47] A. F. Bangura, P. M. C. Rourke, T. M. Benseman, M. Matusiak, J. R. Cooper, N. E. Hussey, and A. Carrington, Phys. Rev. B **82**, 140501 (2010).

[48] W. Tabis, Y. Li, M. Le Tacon, L. Braicovich, A. Kreyssig, M. Minola, G. Dellea, E. Weschke, M. J. Veit, M. Ramazanoglu, A. I. Goldman, T. Schmitt, G. Ghiringhelli, N. Barisic, M. K. Chan, C. J. Dorow, G. Yu, X. Zhao, B. Keimer, and M. Greven, Nat. Commun. **5**, 5875 (2014).

[49] D. van der Marel, Phys. Rev. B **60**, R765 (1999).

[50] Note that only the ratios k_{61}/k_{21} and k_{101}/k_{21} are relevant to our calculations, not the values of these parameters; this is because we are calculating the interlayer conductivity only up to a constant of proportionality, and these parameters do not affect the in-plane conductivity.

[51] To be precise, we fit for the unitless parameters $k_{00}c$ and $k_{40}c$, then obtained values for k_{00} and k_{40} using $c = 2.32$ nm from Analytis *et al.* [36].

[52] A. Nowojewski and S. J. Blundell, Phys. Rev. B **82**, 075121 (2010).

[53] N. E. Hussey, Eur. Phys. J. B **31**, 495 (2003).

[54] A. P. Mackenzie, S. R. Julian, D. C. Sinclair, and C. T. Lin, Phys. Rev. B **53**, 5848 (1996).

[55] H.-Y. Kee and D. Podolsky, Europhys. Lett. **86**, 57005 (2009).

[56] M. Franz, D. E. Sheehy, and Z. Tesanovic, Phys. Rev. Lett. **88**, 257005 (2002).